

Supplementary Information for: 2D vibrational exciton nano-imaging of domain formation in self-assembled monolayers

Thomas P. Gray, Jun Nishida, Samuel C. Johnson, and Markus B. Raschke*

*Department of Physics, Department of Chemistry, and JILA,
University of Colorado, Boulder, CO 80309*

E-mail: markus.raschke@colorado.edu

Materials and Methods

Sample Preparation: 4-nitrothiophenol (4-NTP) and thiophenol were acquired from Sigma-Aldrich. 4-NTP and thiophenol SAMs were prepared by submerging template stripped gold substrates in 20 mL of a 0.1 mM ethanolic solution of 4-NTP or thiophenol for 2 hours.¹ Solutions were used within 3 Days. To remove unbound 4-nitrothiophenol and thiophenol from the substrate surface, substrates were thoroughly rinsed with fresh ethanol for 1 minute and dried with nitrogen gas.² Samples were then measured within two days. Mixed SAMs were prepared using 0.1 mM solutions of 4-NTP and thiophenol in molar ratios varying from 9:1 (90% 4-NTP) to 1:9 (10% 4-NTP).¹

IR *s*-SNOM: IR *s*-SNOM was performed with a tapping mode atomic force microscope (AFM) (customized nanoIR2-s prototype, Anasys Instruments/Bruker) in an asymmetric Michelson interferometer as described previously.^{3,4} 15 mW of tunable femtosecond mid-IR light (Flint, Light Conversion; Levante OPO + HarmoniXX DFG, APE) was attenuated by

$\sim 50\%$ with a mesh filter before reaching the beam splitter (BS) of the Michelson interferometer. In one arm of the Michelson interferometer, an off axis parabolic mirror (OPO) (numerical aperture = 0.45) focused the mid-IR light onto a metalized AFM tip (160AC-GG OPUS, MikroMasch). The femtosecond laser pulse optical frequency was centered on $\bar{\nu}_0$ (1345 cm^{-1}) and had a FWHM bandwidth of $\sim 100\text{ cm}^{-1}$. The tip back scattered light is detected interferometrically with a HgCdTe detector (MCT KLD-0.5-J1/DC/11, Kolmar Technologies). This signal was lock-in demodulated (Zurich Instruments HF2LI) at the second harmonic of the cantilever tapping frequency. Each IR *s*-SNOM spectrum were collected in 50 seconds.

TERS: TERS measurements were performed on a commercial near-field scanning optical microscope (modified OmegaScope-R, Horiba Scientific), whose signal was detected with a qstandard grating spectrometer (iHR320; Horiba Scientific), using 1200 g mm^{-1} under ambient conditions. A protected silver nanoscale tip (Omni-TERS-FM) was brought into contact with the sample and illuminated with a p-polarized 633 nm continuous wave laser that was focused by an objective (100x, 0.7 NA) at an oblique angle of incidence of 65° from surface normal. Spectra were acquired over a 2 second averaging time.

Additional Details on Vibrational Exciton Modeling

The 4-NTP lattice constants of $a = 0.43\text{ nm}$ and $b = 0.37\text{ nm}$ were estimated from known packing densities⁵ and the asymmetry of 4-NTP molecules.

Several approximations of our vibrational exciton model were tested. Disorder could arise from variation in the spacing or tilt of the 4-NTP molecules. Comparing the packing density on Au (111) to the theoretical maximum packing density based on Van der Waals radii of 4-NTP shows that the monolayer is near its density limit. Empty space only leaves room for deviation in 3% of the inter-molecular spacing or 10 degrees of tilt.^{5,6} Additionally, if the 4-NTP and thiophenol are randomly distributed on the gold substrate, then individual

domains will vary stochastically from the solution dilution. Adding pseudorandom Gaussian noise to the position and angles of 4-NTP and sub-selecting the modeled grid from a much larger grid to simulate the effects of these concerns on the model results in a slight broadening of $<0.1 \text{ cm}^{-1}$ and a redshift of $\sim 0.1 \text{ cm}^{-1}$ for grid sizes of 7-50 molecules. While these effects are small, they provide error bars to the model. In addition to physical disorder, coupling between standing-up and lying-down phases was also neglected because the angle between them is large, giving rise to a nearly zero dot products in the transition dipole coupling equations.

Tilt angle of 4-NTP monolayers

STM measurements of 4-NTP monolayers show regions separated by height.⁷ This was interpreted as standing-up and lying-down domains. The presence of standing-up and lying-down domains was later confirmed by ellipsometry and angle-resolved X-ray photoelectron spectroscopy (ARXPS) measurements.² 4-NTP monolayers were observed to be 0.9 nm in height, indicating relatively little tilt in the standing-up domains. However, there are conflicting values in literature for the exact tilt angle θ from the normal axis. Sum-frequency generation and polarization-modulation reflection absorption infrared spectroscopy have placed θ as large as 60° and 66° , respectively.⁸ These methods only produce a single value, likely averaged over both standing-up and lying-down phases, explaining their disagreement from previous close to normal estimation. DFT calculations have placed θ at 33° for standing-up phases and 85° for lying-down phases.⁹ Additionally, STM measurements of a closely related monolayer, 4-Nitrobenzenesulfonyl chloride, have placed its θ at 16° . Due to the uncertainty in exact tilt angle, and for simplicity, $\theta=0^\circ$ was used. For a reasonable value of $\theta = 30^\circ$, $\vec{\mu}_s^\perp$ would need to be increased by 0.03 D from 0.12 D to compensate.

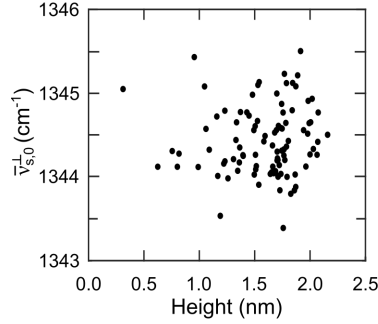


Figure S1: Correlation plot between surface height and $\bar{\nu}_s$ for the 100% 4-NTP SAM from Fig. 2A in the main text. No trend is observed.

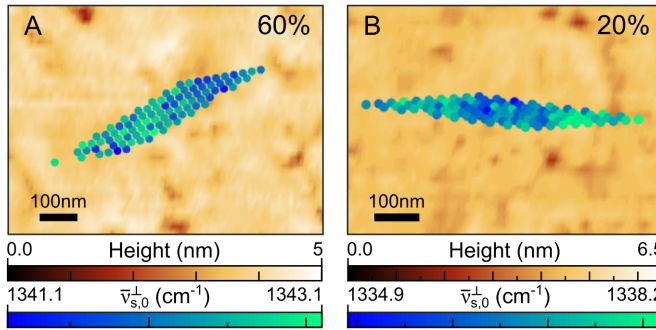


Figure S2: Nanoscale map of spectral variation in $\bar{\nu}_{s,0}^\perp$ in a 60% (A) and 20% (B) 4-NTP monolayer with 15 nm spatial resolution.

Additional *s*-SNOM Experimental Data

To demonstrate that there is no topographic dependence of $\bar{\nu}_{s,0}^\perp$, Fig. S1 contains a correlation plot between the surface height and $\bar{\nu}_{s,0}^\perp$. No correlation between surface height and $\bar{\nu}_{s,0}^\perp$ is observed.

Figure S2 shows spatio-spectral *s*-SNOM images on 60% (A) and 20% (B) 4-NTP SAMs. In the 60% image, variation in $\bar{\nu}_{s,0}^\perp$ of 2 cm^{-1} can be observed, comparable to the 100% 4-NTP case, from $1341.1 \pm 0.2 \text{ cm}^{-1}$ to $1343.1 \pm 0.2 \text{ cm}^{-1}$. The 20% image contains a larger distribution of $\bar{\nu}_{s,0}^\perp$ over 3.3 cm^{-1} from $1334.9 \pm 0.2 \text{ cm}^{-1}$ to $1338.2 \pm 0.2 \text{ cm}^{-1}$.

Figure S3 shows the average spectral phase response for 100% (blue), 60% (red), 20% (green), and 5% (black) spatio-spectral images of mixed 4-NTP and thiophenol monolayers. A clear response can be seen among the 100%, 60%, and 20% spectra, which increases in

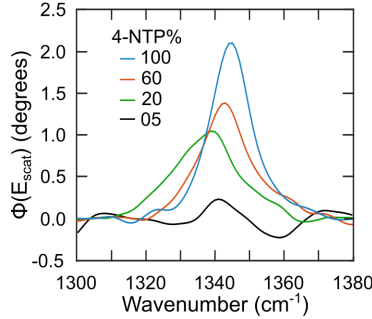


Figure S3: Average spectral phase response for spatio-spectral images of 100% (blue), 60% (red), 20% (green), and 5% (black) 4-NTP monolayers.

amplitude, narrows, and blueshifts with increasing 4-NTP concentration. While the imaginary portion of the spectral response shown in Fig. 2C of the main text demonstrates the narrowing and blueshift of $\bar{\nu}_{s,0}^\perp$, its amplitude is susceptible to changes in local near field enhancement and was therefore normalized. In contrast, the magnitude of the phase response shows a clear dependence on the number of measured nitro groups. The 5% 4-NTP was measured and does show some spectral feature near $\bar{\nu}_s$. It is, however, unclear if this is a real response or just noise.

References

- (1) Dong, L.; Yang, X.; Zhang, C.; Cerjan, B.; Zhou, L.; Tseng, M. L.; Zhang, Y.; Alabastri, A.; Nordlander, P.; Halas, N. J. Nanogapped Au Antennas for Ultrasensitive Surface-Enhanced Infrared Absorption Spectroscopy. *Nano Letters* **2017**, *17*, 5768–5774.
- (2) Jakubowicz, A.; Jia, H.; Wallace, R. M.; Gnade, B. E. Adsorption kinetics of p-nitrobenzenethiol self-assembled monolayers on a gold surface. *Langmuir* **2005**, *21*, 950–955.
- (3) Muller, E. A.; Gray, T. P.; Zhou, Z.; Cheng, X.; Khatib, O.; Bechtel, H. A.; Raschke, M. B. Vibrational exciton nanoimaging of phases and domains in porphyrin nanocrystals. *Proceedings of the National Academy of Sciences* **2020**, *117*, 7030–7037.

- (4) Nishida, J.; Alfaifi, A. H.; Gray, T. P.; Shaheen, S. E.; Raschke, M. B. Heterogeneous Cation–Lattice Interaction and Dynamics in Triple-Cation Perovskites Revealed by Infrared Vibrational Nanoscopy. *ACS Energy Letters* **2020**, *5*, 1636–1643.
- (5) Whelan, C. M.; Smyth, M. R.; Barnes, C. J. HREELS, XPS, and electrochemical study of benzenethiol adsorption on Au(111). *Langmuir* **1999**, *15*, 116–126.
- (6) Wan, L.-J.; Terashima, M.; Noda, H.; Osawa, M. Molecular Orientation and Ordered Structure of Benzenethiol Adsorbed on Gold(111). *The Journal of Physical Chemistry B* **2000**, *104*, 3563–3569.
- (7) Nielsen, J. U.; Esplandiu, M. J.; Kolb, D. M. 4-nitrothiophenol SAM on Au(111) investigated by in situ STM, electrochemistry, and XPS. *Langmuir* **2001**, *17*, 3454–3459.
- (8) Cecchet, F.; Lis, D.; Guthmuller, J.; Champagne, B.; Fonder, G.; Mekhalif, Z.; Caudano, Y.; Mani, A. A.; Thiry, P. A.; Peremans, A. Theoretical Calculations and Experimental Measurements of the Vibrational Response of p-NTP SAMs: An Orientational Analysis. *The Journal of Physical Chemistry C* **2010**, *114*, 4106–4113.
- (9) Sun, J. J.; Su, H. S.; Yue, H. L.; Huang, S. C.; Huang, T. X.; Hu, S.; Sartin, M. M.; Cheng, J.; Ren, B. Role of Adsorption Orientation in Surface Plasmon-Driven Coupling Reactions Studied by Tip-Enhanced Raman Spectroscopy. *Journal of Physical Chemistry Letters* **2019**, *10*, 2306–2312.